

Observation of the decay mode $K_L^0 \rightarrow \gamma\gamma ee$

W. M. Morse, L. B. Leipuner, R. C. Larsen, and E. Jastrzembski*
Physics Department, Brookhaven National Laboratory, Upton, New York 11973

R. K. Adair, H. B. Greenlee,[†] H. Kasha, E. B. Mannelli,[‡] K. E. Ohl, M. P. Schmidt, and
 M. R. Vagins
Physics Department, Yale University, New Haven, Connecticut 06511

C. B. Schwarz
Department of Physics and Astronomy, Vassar College, Poughkeepsie, New York 12601

(Received 21 May 1990; revised manuscript received 29 August 1991)

Results of a search for the decay mode $K_L^0 \rightarrow \gamma\gamma ee$ ($K_L^0 \rightarrow \gamma ee$ with a hard internal bremsstrahlung) are reported. The measured branching ratio is $(6.6 \pm 3.2) \times 10^{-7}$, in agreement with the QED prediction of 5.8×10^{-7} . The infrared cutoff for both branching ratios is the requirement that both photons have an energy of at least 5 MeV on the center of mass.

PACS number(s): 13.40.Hq, 12.20.Fv, 13.20.Eb

The rare process $K_L^0 \rightarrow \gamma\gamma ee$ is a potentially serious background in experiments searching for the still rarer process $K_L^0 \rightarrow \pi^0 ee$. BNL experiment 845 was undertaken primarily to search for the latter decay mode. The results of that search were negative and have been described elsewhere [1]. QED predictions for the background process $K_L^0 \rightarrow \gamma\gamma ee$ and the implications for $K_L^0 \rightarrow \pi^0 ee$ experiments have been considered in a separate paper [2]. It was pointed out in that paper that current $K_L^0 \rightarrow \pi^0 ee$ experiments may have enough sensitivity to see the decay mode $K_L^0 \rightarrow \gamma\gamma ee$. This paper reports the results of a search for $K_L^0 \rightarrow \gamma\gamma ee$ by BNL E-845 [3].

A detailed description of the E-845 detector and neutral beam can be found in Ref. [1]. A diagram of the experiment is shown in Fig. 1. The momenta of charged particles were determined using a charged particle spectrometer consisting of four drift chambers (A, B, C, D) and a dipole analyzing magnet with a p_T kick of 114 MeV/c. A lead glass electromagnetic calorimeter consisting of 244 fiducial lead-glass blocks was used to measure the energy and position of electrons and photons. Additional electron identification was provided by an atmospheric pressure hydrogen threshold Čerenkov counter (pion threshold 8 GeV/c) and a muon-pion filter following the lead glass. The muon-pion filter consisted of 15 cm of lead followed by a scintillation counter array (G). The total amount of material in front of the G array (lead and lead glass) was 47 radiation lengths, but only

about 2 interaction lengths, so that pions or pion-induced hadronic showers had a significant probability of reaching the G array. Photon vetoes (V) consisting of 3 radiation lengths of material followed by scintillation counters framed the acceptance at the downstream end of the decay region and around the outside of the lead glass. Two scintillation counter arrays (F and E) were used for triggering.

The neutral beam was produced by the interaction of a 24-GeV primary proton beam with a one interaction length copper target, followed by a series of collimators and sweeping magnets. The upstream end of the 6-m-long evacuated decay region was located 10 m from the production target. The energy range of detected K_L^0 decays was from 4 to about 20 GeV. The trigger counter arrays, lead glass, and muon-pion filter had holes for the neutral beam to pass through. The drift chambers did

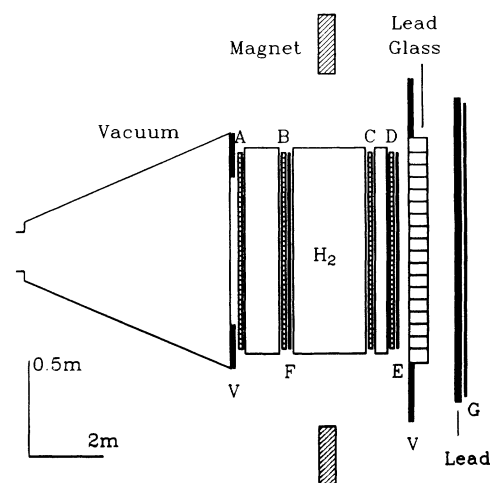


FIG. 1. Plan view of the E-845 detector.

*Present address: CEBAF, Newport News, VA 23606.

[†]Present address: Fermi National Accelerator Laboratory, Batavia, IL 60510.

[‡]Present address: INFN Sezione di Pisa, Via Livornese, 582/A, S. Piero a Grado, 56010 Pisa, Italy.

not have holes and were active in the beam region.

The trigger requirements for most of the data were that there be two identified electrons and at least 4 GeV of energy deposited in the lead glass. Trigger level electron identification required hits in the same quadrant in the E counter array and the Čerenkov counter and at least 1 GeV of energy deposited in the lead-glass quadrant. Hits were not allowed in the veto counters or in the same quadrant of the G array as an electron. In addition to the electron trigger, there was a prescaled minimum bias two-charged-particle trigger that used only the F and E counters. Minimum bias triggers were collected throughout the experiment with a prescale factor of 10 000. The minimum-bias data contained large numbers of the decays $K_L^0 \rightarrow \pi^+ \pi^- \pi^0$ and $K_L^0 \rightarrow \pi e \nu$. The former were used to normalize the experiment. The latter were used to study electron identification.

The experimental signature for $K_L^0 \rightarrow \gamma\gamma ee$ is very similar to $K_L^0 \rightarrow \pi^0 ee$. The only observable difference between these two decay modes is the invariant mass of the photon pair. The analysis method used in the search for $K_L^0 \rightarrow \gamma\gamma ee$ was kept as similar as possible to the one used for $K_L^0 \rightarrow \pi^0 ee$. The basic requirements for both searches were that there be a pair of opposite sign electron tracks and two neutral lead glass clusters kinematically consistent with $K_L^0 \rightarrow \pi^0 ee$ or $K_L^0 \rightarrow \gamma\gamma ee$. Electron tracks were required to come from a common vertex in the fiducial decay region. Electron identification was performed by requiring that there be an in-time Čerenkov counter hit in the proper quadrant and that the track be associated with an in-time lead glass cluster whose energy was consistent with the measured track momentum ($0.75 < E/p < 1.25$). The Čerenkov counter was measured to have an efficiency of 92%. Photons were required to be in time and to have an energy greater than 500 MeV (700 MeV next to the beam hole to suppress backgrounds from beam halo interactions in the lead glass). The vector momentum of photons was reconstructed assuming that they originated at the charged-particle vertex. Electron and photon lead glass clusters were required to pass a shape cut (i.e., they had to have a narrow profile). Finally, events with extra in-time particles (defined as drift-chamber tracks and/or lead glass clusters) were vetoed.

The following kinematic cuts were used in the $K_L^0 \rightarrow \pi^0 ee$ search:

$$|m_{\gamma\gamma} - m_{\pi^0}| < 33 \text{ MeV} , \quad (1)$$

$$|m_{\pi^0 ee} - m_{K^0}| < 32 \text{ MeV} , \quad (2)$$

$$\theta_K^2 < 12 \text{ mrad}^2 , \quad (3)$$

$$m_{ee} > 145 \text{ MeV} , \quad (4)$$

where θ_K^2 is the square of the target angle (i.e., the angle between the reconstructed kaon momentum and a line joining the production target and the decay vertex in the laboratory). The cut on m_{ee} was made to eliminate backgrounds from π^0 Dalitz decay ($\pi^0 \rightarrow \gamma ee$). Except for this constraint on m_{ee} , these are three standard deviation cuts, based on expected experimental resolutions for the

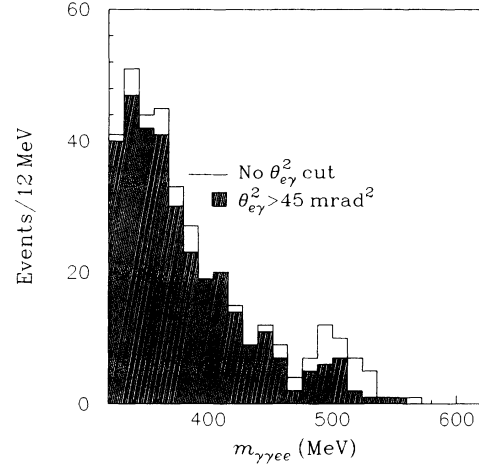


FIG. 2. $\gamma\gamma ee$ effective mass with and without external bremsstrahlung cut.

unobserved decay mode $K_L^0 \rightarrow \pi^0 ee$. For the $K_L^0 \rightarrow \gamma\gamma ee$ search the kinetic cuts were modified as

$$|m_{\gamma\gamma ee} - m_{K^0}| < 46 \text{ MeV} , \quad (5)$$

$$\theta_K^2 < 12 \text{ mrad}^2 , \quad (6)$$

$$m_{ee} > 100 \text{ MeV} . \quad (7)$$

The π^0 mass cut was eliminated and the cut on the total invariant mass was widened. The $\gamma\gamma ee$ mass resolution is worse than the $\pi^0 ee$ mass resolution because in the former case there is no constraint on the $\gamma\gamma$ invariant mass. In addition, the cut on m_{ee} was reduced. This reduction increased the $K_L^0 \rightarrow \gamma\gamma ee$ acceptance at the cost of admitting events arising from π^0 Dalitz decay.

The line histogram in Fig. 2 shows the $\gamma\gamma ee$ effective mass distribution for those events satisfying all of the above requirements (except for the cut on $m_{\gamma\gamma ee}$ itself). There is a clear peak at the kaon mass resulting from $K_L^0 \rightarrow \gamma ee$ decays with an additional photon from either internal or external bremsstrahlung. In order to isolate those events arising from internal bremsstrahlung, a constraint on the angle between photons and electrons was imposed. Figure 3 shows the distribution of the square of the laboratory angle ($\theta_{e\gamma}$) between photons and the electron in K_{e3} events. There is a strong peak at $\theta_{e\gamma}^2 = 0$. In both the $K_L^0 \rightarrow \pi^0 ee$ and $K_L^0 \rightarrow \gamma\gamma ee$ searches, photons were required to satisfy the approximately three standard deviation cut $\theta_{e\gamma}^2 > 45 \text{ mrad}^2$ ($\theta_{e\gamma} > 6.7 \text{ mrad}$). This bremsstrahlung cut was much more effective against external bremsstrahlung than against internal bremsstrahlung. The number of radiation lengths upstream of the spectrometer magnet was 0.0153. In a typical $K_L^0 \rightarrow \gamma ee$ event, there is a probability of about 5% that one of the two electrons will generate an external bremsstrahlung photon with a laboratory energy greater than 500 MeV. The probability of hard internal bremsstrahlung is similar. Typical laboratory angles of external bremsstrahlung photons are $\theta_{e\gamma} \approx 1/\gamma$, where $\gamma > 2000$ for accepted electrons. External bremsstrahlung at wider

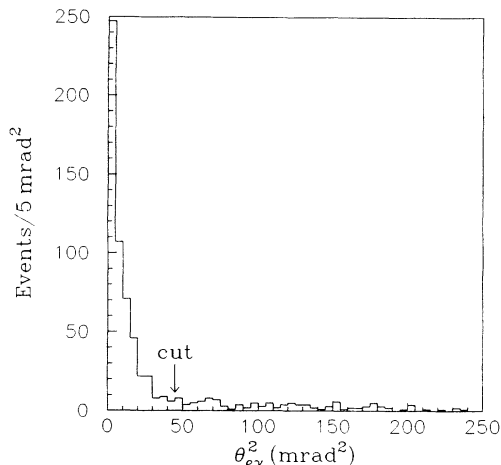


FIG. 3. Histogram of the square of the angle between photons and the electron in K_{e3} events. The bremsstrahlung cut is shown.

angles falls off as $\theta_{e\gamma}^{-4}$. However, the angular distribution of internal bremsstrahlung falls off only as $\theta_{e\gamma}^{-2}$ (in the laboratory as well as in the e^+e^- center of mass) and has a significant wide angle tail as well. Figure 4 shows the laboratory angular distribution of internal bremsstrahlung photons in Monte Carlo generated $K_L^0 \rightarrow \gamma\gamma ee$ events, where only the smallest of the four combinatoric values of $\theta_{e\gamma}^2$ was kept for each Monte Carlo event. The bremsstrahlung cut reduced external bremsstrahlung to a negligible level and lowered the acceptance for $K_L^0 \rightarrow \gamma\gamma ee$ by 45%.

The shaded histogram in Fig. 2 indicates the events which remain after the $\theta_{e\gamma}^2$ cut is applied. There is still a peak at the kaon mass, although it has been significantly reduced as expected. The background is not significantly affected, also as expected. The background events in the low-mass region are primarily from $K_{\pi 3}$ decays with one or two π^0 Dalitz decays where all the decay products are not observed. One other source of background is from

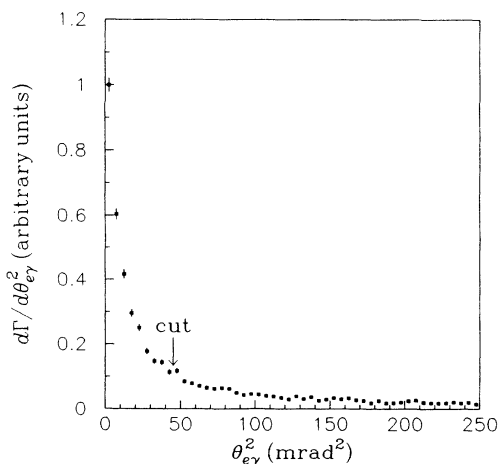


FIG. 4. Histogram of the square of the angle between photons and electrons in Monte Carlo $K_L^0 \rightarrow \gamma\gamma ee$ events. The bremsstrahlung cut is shown.

K_{e3} decays where the charged pion is misidentified as an electron and two additional photons come from any of the following sources: internal bremsstrahlung, fragmentation of the charged pion lead glass cluster, and accidentals. These events have an approximately flat distribution in mass over the region of interest.

There are 30 events in Fig. 2 which satisfy $\theta_{e\gamma}^2 > 45$ mrad^2 and $|m_{\gamma\gamma ee} - m_{K^0}| < 46$ MeV. However, a non-trivial fraction of these events are from the sources described above. It was therefore necessary to perform a background subtraction. A fairly simple way to estimate the background is to consider events which have larger θ_K^2 . Figure 5 shows the $\gamma\gamma ee$ effective mass plot for events with $\theta_K^2 < 12$ mrad^2 (line) and events with $12 < \theta_K^2 < 24$ mrad^2 (shaded). There are 10 events satisfying $|m_{\gamma\gamma ee} - m_{K^0}| < 46$ MeV in the latter distribution. The background in the signal region can be estimated by scaling this value by 1.22. The scale factor represents the ratio of the number of events with small θ_K^2 to the number with large θ_K^2 satisfying $320 \text{ MeV} < m_{\gamma\gamma ee} < (m_{K^0} - 46 \text{ MeV})$. [This corresponds to a range just below the signal region defined by Eq. (5)]. Using this method the number of signal events is $30 - 12.2 = 17.8$ events.

In practice, a more complicated procedure was used to determine the background level. This method takes into account that the two main types of backgrounds behave differently as a function of effective mass. First, the amount of flat background was found by studying a region in $\gamma\gamma ee$ effective mass and θ_K^2 populated with K_{e3} events. Specifically, the region $30 \text{ mrad}^2 < \theta_K^2 < 100 \text{ mrad}^2$ and $545 \text{ MeV} < m_{K^0} < 600 \text{ MeV}$ was considered, leading to an estimated background from K_{e3} decays of 2.6 ± 0.8 events/ $\text{mrad}^2 \text{ GeV}$. To determine the amount of background from Dalitz decay, the ratio of the two histograms in Fig. 2 (after the flat background has been subtracted from both) was fit for the effective-mass range $320 < m_{\gamma\gamma ee} < 450$ MeV. The result of this fit was used to extrapolate the ratio into the signal region, and hence calculate the amount of Dalitz background with $\theta_K^2 < 12$ mrad^2 from the number of events with $12 < \theta_K^2 < 24$

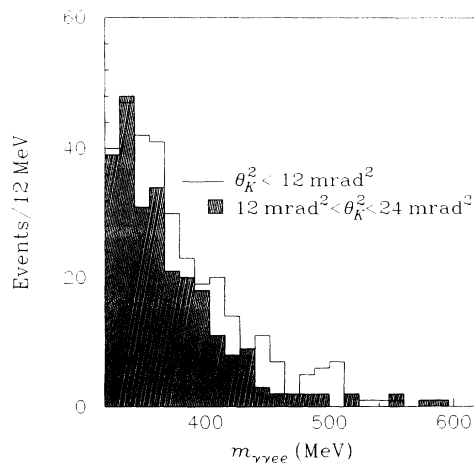


FIG. 5. $\gamma\gamma ee$ effective mass for different values of θ_K^2 . The external bremsstrahlung cut has been applied.

mr 2 . (The efficacy of this approach was checked using events satisfying $24 < \theta_K^2 < 36$ mr 2 to predict the number of events with $12 < \theta_K^2 < 24$ mr 2). The final result of this procedure was an estimated background from both sources of 13.28 ± 5.93 events. (There are 10.41 events from the Dalitz background and 2.87 events from the K_{e3} background.) Note that the probability of observing 30 events when 13.28 are expected is less than 1%. The signal is 16.72 ± 8.07 events. The error is statistical and includes the error from the fitting procedure. This signal value is in good agreement with the result of the simple scaling estimate described above.

The $K_L^0 \rightarrow \gamma\gamma ee$ acceptance was determined using a Monte Carlo simulation based on the program described in Ref. [2]. Unlike the Monte Carlo results presented in Ref. [2], the results in this paper include a simulation of the E-845 detector. In this paper a single infrared cutoff is consistently used. The minimum center-of-mass energy (apart from resolution smearing) that a photon must have to be accepted by the E-845 detector is 6.2 MeV (i.e., a 500-MeV photon from a 20-GeV kaon). The requirement that both photons in $K_L^0 \rightarrow \gamma\gamma ee$ have at least 5 MeV in the center of mass has been adopted as a standard infrared cutoff.

The Monte Carlo calculation of the decay $K_L^0 \rightarrow \gamma\gamma ee$ is affected by various theoretical and experimental uncertainties. Theoretical uncertainties include a 4% error of the measured branching ratio for $K_L^0 \rightarrow \gamma\gamma$, [4] and uncertainty in the K_L^0 - γ - γ form factor [5]. The latter uncertainty contributes a 1.6% to the error of the predicted branching ratio for $K_L^0 \rightarrow \gamma\gamma ee$ and a 4.2% error to the calculated acceptance. In addition to the theoretical uncertainties, a 6% systematic error was assigned to the overall normalization of the experiment.

With the cuts described above, the E-845 detector has an acceptance for $K_L^0 \rightarrow \gamma\gamma ee$ of 2.2×10^{-4} . Using the same normalization as Ref. [1], the single-event branching ratio sensitivity is $(3.95 \pm 0.29) \times 10^{-8}$. Using this value along with a signal of 16.72 ± 8.07 events, the result is $B(K_L^0 \rightarrow \gamma\gamma ee) = (6.6 \pm 3.2) \times 10^{-7}$. This is in good agreement with the predicted branching ratio [2] of $(5.81 \pm 0.25) \times 10^{-7}$.

This analysis can be checked using a set of cuts devised to extract the signal from the background more clearly. The first cut made to further isolate the signal was to require

$$m_{ee} > 145 \text{ MeV} . \quad (8)$$

Increasing this constraint from 100 MeV reduced the $K_L^0 \rightarrow \gamma\gamma ee$ acceptance by 21%, while eliminating backgrounds from the Dalitz decay of a single π^0 . There are 15 events in the signal region defined by Eqs. (5) and (6) satisfying $m_{ee} > 145$ MeV.

One remaining source of background for $K_L^0 \rightarrow \gamma\gamma ee$ is $K_L^0 \rightarrow \pi^0 \pi^0 \pi^0$ where two final-state photons (from different π^0 's) undergo highly asymmetric external or internal pair conversion. This background has missing energy since two of the four final-state electrons must remain undetected. There are also two extra photons which must either escape without much energy or merge

with other photon or electron clusters in the lead glass. This background was discriminated against using a kinetic cut. The center-of-mass energy of an electron E_e^* from $K_L^0 \rightarrow \pi^0 \pi^0 \pi^0$ has a maximum of about 165 MeV. The $K_L^0 \rightarrow \pi^0 \pi^0 \pi^0$ double conversion background was eliminated by requiring one of the two electrons in $K_L^0 \rightarrow \gamma\gamma ee$ events to satisfy

$$E_e^* > 165 \text{ MeV} . \quad (9)$$

This cut lowered the $K_L^0 \rightarrow \gamma\gamma ee$ acceptance by 34% while effectively eliminating the background from $K_L^0 \rightarrow \pi^0 \pi^0 \pi^0$. The number of events in the signal region was reduced from 15 to 9. Under the assumption that the cuts defined by Eqs. (8) and (9) eliminate all of the Dalitz background and 48% of the $K_L^0 \rightarrow \gamma\gamma ee$ signal, the expected number of events in the signal region is 11.6, in agreement with the actual number of events observed.

Note that the double conversion background from $K_L^0 \rightarrow \pi^0 \pi^0$ is sufficiently rare so that it is not a problem. The branching ratio for $\pi^0 \rightarrow \gamma ee$ is 1.20%. The possibility of external conversion before the first drift-chamber plane increases this to an effective branching ratio of 1.65%. The effective branching ratio for $K_L^0 \rightarrow \pi^0 \pi^0$ with two photon conversions is then $(9.1 \times 10^{-4})(0.0165)^2 = 2.5 \times 10^{-7}$. This branching ratio is no larger than the predicted branching ratio for $K_L^0 \rightarrow \gamma\gamma ee$. The kinematic cuts and the requirement that the extra charged particles not be visible reduce the $K_L^0 \rightarrow \pi^0 \pi^0$ background to a negligible level compared to $K_L^0 \rightarrow \gamma\gamma ee$. Studies of the charged mode $K^0 \rightarrow \pi^+ \pi^-$ have shown that $K_S^0 \rightarrow \pi^0 \pi^0$ is small compared to $K_L^0 \rightarrow \pi^0 \pi^0$, and hence $K_S^0 \rightarrow \pi^0 \pi^0$ is not a significant background either.

The major remaining background is from K_{e3} decays. This background was studied by identifying events from minimum bias data containing a pion, an electron, and two photons. (The constraints on photon time were removed for this study.) The e^+e^- effective mass of these events was then calculated assuming both particles were electrons. The m_{ee} distribution is shown as the line histogram in Fig. 6 for those events which satisfy the kinemat-

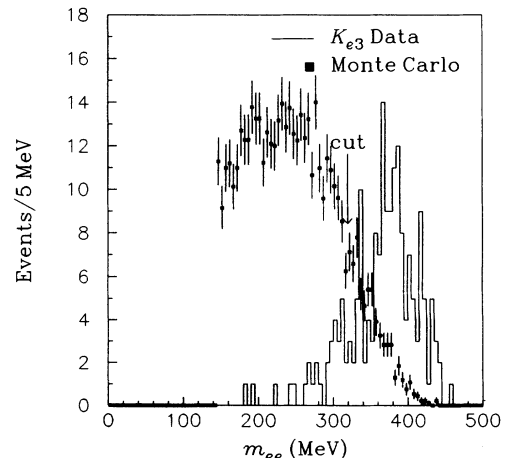


FIG. 6. Histogram of e^+e^- invariant mass for K_{e3} background events and Monte Carlo $K_L^0 \rightarrow \gamma\gamma ee$ events.

ic constraints defined by Eqs. (5), (6), and (9). The bias toward high mass is a feature of K_{e3} associated backgrounds. Also shown in Fig. 6 is the expected Monte Carlo e^+e^- invariant-mass distribution for $K_L^0 \rightarrow \gamma\gamma ee$ events. The cut $m_{ee} < 320$ MeV was applied. This cut eliminates 83% of K_{e3} distribution while lowering the $K_L^0 \rightarrow \gamma\gamma ee$ acceptance by only 14%. The number of events in the signal region was reduced from 9 to 5. The expected number of remaining events is 8.0.

Finally, a number of minor cuts were made to further suppress K_{e3} accidentals. If a pion cluster merges with an accidental cluster, the pion can satisfy the lead-glass energy requirements and possibly be misidentified as an electron. To discriminate against this and in general improve π/e rejection, the electron cluster shape cut was tightened. The mean-square width of electron clusters is defined as

$$w^2 = \frac{\sum_i (\Delta x_i^2 + \Delta y_i^2) E_i}{\sum_i E_i}, \quad (10)$$

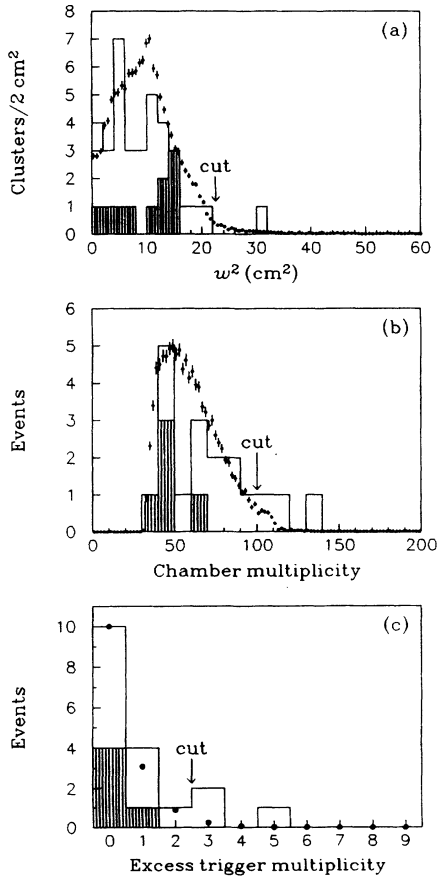


FIG. 7. Nonkinematic cuts: (a) electron cluster mean-square width; (b) drift-chamber multiplicity; (c) excess trigger counter multiplicity. The histograms represent the 18 events remaining after the kinematic cuts have been applied which satisfy $300 \text{ MeV} < m_{\gamma\gamma ee} - m_{K^0} < 700 \text{ MeV}$ and $\theta_K^2 < 100 \text{ mrad}^2$. The shaded area of each histogram represents the final sample of 5 events. The points are fiducial distributions as measured in minimum-bias (a) $K_L^0 \rightarrow \pi e \nu$ and (b), (c) $K_L^0 \rightarrow \pi^+ \pi^- \pi^0$ data.

where E_i is the energy of lead glass block i and Δx_i and Δy_i are the transverse displacements of the lead-glass block i relative to the extrapolated position of the drift chamber track at the lead glass. The effect of the tightened shape cut is shown in Fig. 7(a) where the 18 events remaining in the wide kinematic range $300 \text{ MeV} < m_{\gamma\gamma ee} - m_{K^0} < 700 \text{ MeV}$ and $\theta_K^2 < 100 \text{ mrad}^2$ are shown as the line histogram, and the 5 events in the signal region are shaded. Also shown is a fiducial distribution measured from K_{e3} electrons. The two distributions are normalized by maximum. The cut on w^2 was made at the approximate value where the data histogram is twice the fiducial distribution. This corresponds to $w^2 = 22.6 \text{ cm}^2$. (The value used in the $K_L^0 \rightarrow \pi^0 ee$ analysis was 32.3 cm^2 .) The shape cut has a relative efficiency of 98.2% per electron. To suppress accidentals and beam interactions generally, events with more than 100 total drift chamber hits (efficiency 97.7% for $K_L^0 \rightarrow \pi^+ \pi^- \pi^0$) were eliminated. The effect of this requirement is shown in Fig. 7(b) where again the cut is at the approximate place where the fiducial histogram is half the data. Finally, events with more than two non-track-associated, in-time trigger counters (efficiency 97.6% for $K_L^0 \rightarrow \pi^+ \pi^- \pi^0$ events) were eliminated. The effect of this cut is shown in Fig. 7(c). The total efficiency of all of the nonkinematic cuts was 92.0%. After all the cuts were applied there are 12 events remaining in the wide kinematic range, of which 5 are in the signal region. Distributions in $m_{\gamma\gamma ee}$ and θ_K^2 distributions are shown in Fig. 8 for data and the Monte

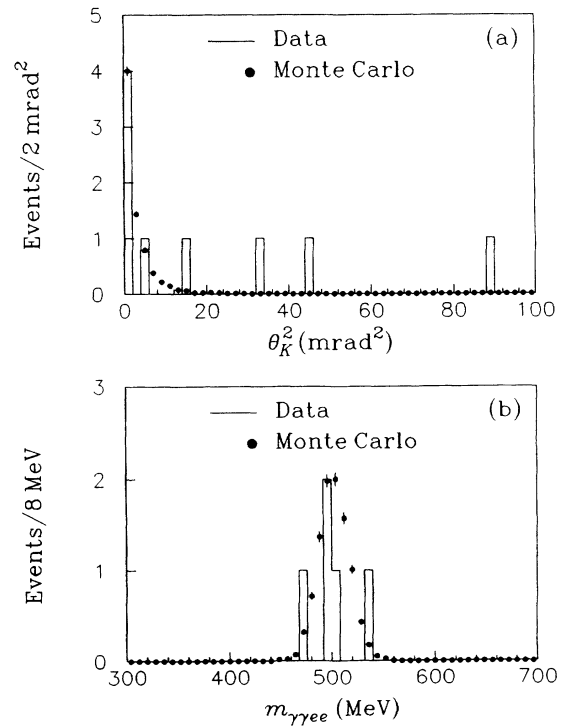


FIG. 8. Histogram of (a) θ_K^2 and (b) $m_{\gamma\gamma ee}$ for data and the Monte Carlo simulation using final cuts.

Carlo simulation. From these plots a background of 0.5 ± 0.5 events was estimated. The total efficiency of all of the extra cuts is 41%. With a signal of 4.5 events the branching ratio result is $(4.4 \pm 2.2) \times 10^{-7}$, in good agreement with the value obtained from the less restrictive analysis.

In conclusion, we have observed the decay $K_L^0 \rightarrow \gamma\gamma ee$. We quote as a final result the value $B(K_L^0 \rightarrow \gamma\gamma ee) = (6.6 \pm 3.2) \times 10^{-7}$ obtained from our less restrictive analysis. This result is in agreement with the QED prediction of 5.81×10^{-7} .

We would like to thank the staff of the Brookhaven AGS for their support in the construction and operation of E-845. We thank M. Lenz and J. Yelk for technical contributions to the experiment. We thank M. Mannelli and S. F. Schaffner for contributions to E-845 resulting from their efforts on an earlier experiment (E-780). This research was supported by the U.S. Department of Energy under Contracts No. DE-AC02-76ER03075 and No. DE-AC02-76CH00016. One of us (M.P.S.) has received additional financial support from the Alfred P. Sloan Foundation.

[1] K. E. Ohl *et al.*, Phys. Rev. Lett. **64**, 2755 (1990).

[2] H. B. Greenlee, Phys. Rev. D **42**, 3724 (1990). The Monte Carlo calculations discussed in this reference were based on the program described in L. Roberts and J. Smith, *ibid.* **33**, 3457 (1986).

[3] The analysis presented in this paper supersedes the results

discussed in W. M. Morse *et al.*, Yale University, Report No. YAUG-A-90/4, 1990 (unpublished).

[4] Particle Data Group, G. P. Yost *et al.*, Phys. Lett. B **204**, 1 (1988).

[5] K. E. Ohl *et al.*, Phys. Rev. Lett. **65**, 1407 (1990).

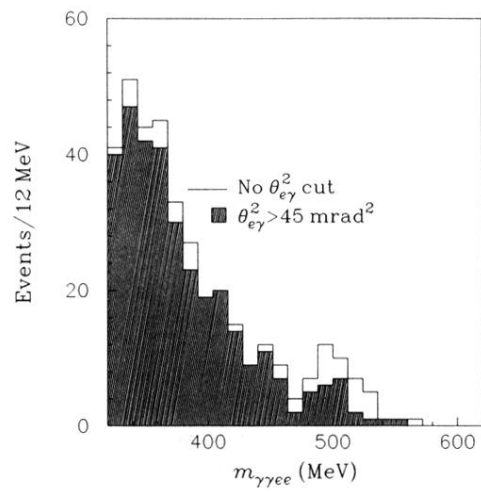


FIG. 2. $\gamma\gamma ee$ effective mass with and without external bremsstrahlung cut.

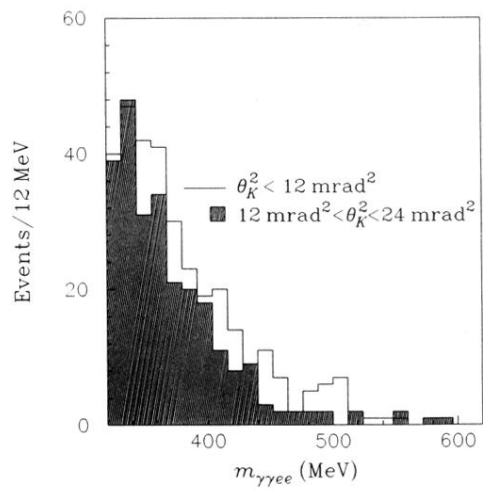


FIG. 5. $\gamma\gamma ee$ effective mass for different values of θ_k^2 . The external bremsstrahlung cut has been applied.